ARTICLE OPEN

Check for updates

pNaktide reverses metabolic reprogramming and disease progression of ATP1A1-deficiency clear cell renal cell carcinoma

Yinghong Zhao[1,3], Jialing Lv[1,3], Wen Zhang[1], Ruoyu Deng[1], Chunyan Li[1], Lin Wang[1], Tengfei Zhang[1], Feineng Liu[1], Kaili Ma[2]✉, Zhengcun Wu[2]✉ and Chao Zhang[1]✉

ATP1A1 has been reported to exhibit differential expression across various tumors; however, its specific role in clear cell renal cell carcinoma (ccRCC) remains uncharted. This study investigates the role of *ATP1A1* in ccRCC, assessing its potential as a prognostic marker and therapeutic target. Through database analysis and clinical sample evaluation, we found that *ATP1A1* expression is significantly downregulated in ccRCC and closely correlates with poor patient prognosis. Both in vitro and in vivo experiments further confirmed that *ATP1A1* exerts tumor-suppressive effects by inhibiting SRC kinase activity. Additionally, co-expression gene analysis suggests that *ATP1A1* may regulate ccRCC development by targeting metabolic reprogramming. We also discovered that the overexpression of *ATP1A1* induces a metabolic shift from glycolysis to oxidative phosphorylation (OXPHOS), resulting in increased levels of reactive oxygen species (ROS) and subsequent apoptosis. Moreover, we evaluated the therapeutic potential of pNaktide, a peptide that mimics *ATP1A1* function. Our research indicates that pNaktide effectively inhibits ccRCC proliferation both in vitro and in vivo by suppressing the SRC signaling pathway and inducing metabolic changes akin to those observed with *ATP1A1* overexpression. Studies utilizing nude mouse models further confirmed that pNaktide significantly reduces tumor volume and weight, supporting its potential as a therapeutic agent. In summary, this study demonstrates that low *ATP1A1* expression is a critical factor in ccRCC progression and that pNaktide, by restoring *ATP1A1*-like functions, presents a promising therapeutic strategy for ccRCC.

Cancer Gene Therapy; https://doi.org/10.1038/s41417-025-00971-z

Graphical Abstract

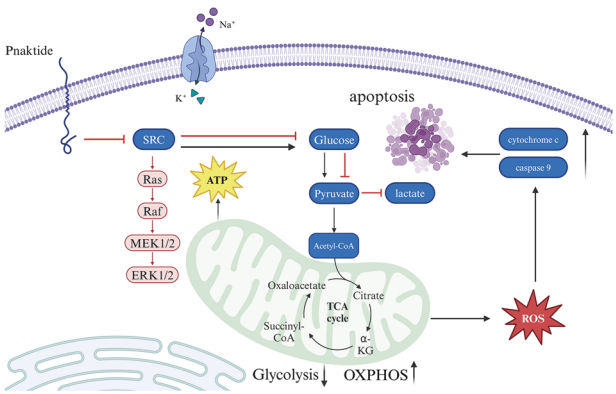

INTRODUCTION

Clear cell renal cell carcinoma (ccRCC) is the most prevalent and aggressive subtype of renal cancer, accounting for approximately 80% of all renal cell cancer cases. The 5-year survival rate for ccRCC is a mere 5%, with long-term survivors rarely achieving a definitive cure [1]. According to estimates by the American Cancer Society, approximately 79,000 new cases of kidney cancer will be diagnosed in the United States in 2022, with ccRCC being the most common subtype [2]. At the molecular level, ccRCC is characterized by deregulated hypoxia-inducible factor signaling, mutations in several key chromatin-modifying enzymes, and numerous alterations in cellular metabolism [3]. Approximately

[1]Department of Oncology, The First People's Hospital of Qujing/The Qujing Affiliated Hospital of Kunming Medical University, Qujing, China. [2]Institute of Medical Biology, Chinese Academy of Medical Sciences & Peking Union Medical College, Kunming, China. [3]These authors contributed equally: Yinghong Zhao, Jialing Lv. ✉email: mklpumc@gmail.com; wzc1121@imbcams.com.cn; zhangchao@kmmu.edu.cn

Received: 16 April 2025 Revised: 5 September 2025 Accepted: 25 September 2025
Published online: 07 October 2025

30% of patients present with metastatic disease at the time of diagnosis [4]. Early-stage ccRCC is preferably treated with surgical intervention, while advanced ccRCC typically relies on chemotherapy or molecular-targeted therapy. However, these treatments exhibit suboptimal efficacy, resulting in low overall survival (OS) rates. Therefore, identifying highly specific diagnostic and therapeutic molecular targets is crucial for improving the prognosis and survival of patients with ccRCC.

α1 Na^+/K^+-ATPase (NKA), encoded by *ATP1A1*, is a membrane-embedded channel protein with ATPase activity that plays a crucial role in active transport, energy metabolism, and signal transduction [5, 6]. Recent studies have demonstrated that aberrant expression of *ATP1A1* is prevalent in various tumors, with its tissue-specific expression linked to cancer development [7–13]. In renal cell carcinoma (RCC), low levels of *ATP1A1* expression correlate with reduced patient survival, while increasing its expression can significantly extend the survival time of RCC patients [14, 15]. Overexpression of the *ATP1A1* gene in RCC cells markedly inhibits cell proliferation by enhancing reactive oxygen species (ROS) production and inducing apoptosis [14]. However, the specific functions and mechanisms of *ATP1A1* in ccRCC remain incompletely understood.

The NKA α1-SRC complex serves as a pivotal element in NKAα1-mediated signal transduction [16]. SRC, a non-receptor tyrosine kinase, plays a significant role in regulating cell proliferation, apoptosis, migration, and invasion, and is implicated in the progression of various cancers. Research has identified two potential interaction domains between NKA α1 and SRC [17]. Studies indicate that the interaction of NKA α1 inhibits SRC phosphorylation, thereby modulating the downstream signaling cascades associated with SRC, including PI3K, RAS/RAF/ERK, and PLC/PKC, which are critical for cell proliferation, differentiation, and apoptosis [18]. In specific cancer cells, the downregulation of NKA may lead to an increase in SRC kinase activity; consequently, the supplementation of NKA or its analogs could inhibit tumor growth by antagonizing this kinase activity [17].

Our analysis of data from the TCGA database concerning ccRCC samples revealed a significant reduction in *ATP1A1* expression, accompanied by a notable increase in SRC levels. Given the critical role of SRC signaling in the development of ccRCC, we hypothesized that the activation of SRC signaling, regulated by Na^+/K^+ ATPase (NKA), could represent a promising therapeutic strategy for ccRCC. To validate this hypothesis, we evaluated the role of *ATP1A1* in ccRCC proliferation and its regulatory influence on the SRC signaling pathway. Additionally, we investigated pNaktide, a 20-amino-acid peptide designed to target the binding region between the α1 subunit of NKA and SRC kinase, which functions as an SRC kinase inhibitor. We propose that pNaktide may act as a substitute for NKA, thereby inhibiting ccRCC proliferation by counteracting SRC kinase activity. To further explore this hypothesis, we assessed whether pNaktide could diminish the SRC activity and its downstream effectors in ccRCC cells. This investigation could provide a novel therapeutic approach to mitigate SRC pathway activation resulting from reduced *ATP1A1* expression in ccRCC.

MATERIALS AND METHODS

Data analysis

The clinical data of ccRCC were obtained from the TCGA (Firehose Legacy) dataset through the GEPIA2 (http://gepia2.cancer-pku.cn/) [19] and UALCAN (http://ualcan.path.uab.edu/) platforms [20]. This dataset encompasses information on OS, disease-specific survival (DSS), and progression-free interval (PFI) related to *ATP1A1* expression. Tissue microarray chips containing adjacent non-tumor tissues and primary ccRCC tissues were acquired from Servicebio (Wuhan, China). The correlations between *ATP1A1* expression and oxidative phosphorylation-related genes were analyzed using Pearson linear regression, with statistical significance determined via the Benjamini-Hochberg correction. All computations were conducted using the R language (version 4.2.1).

Co-expression gene analysis

Genes co-expressed with *ATP1A1* were identified using the UALCAN database. These genes were subsequently utilized to construct a protein-protein interaction (PPI) network employing either the STRING database (https://string-db.org) or Cytoscape software. Within the constructed PPI network, hub genes were identified by calculating various topological parameters, including node degree, betweenness centrality, and closeness centrality for each gene. The Kyoto Encyclopedia of Genes and Genomes (KEGG) pathway enrichment analysis [21] and Gene Ontology (GO) enrichment analysis [22] were performed on the identified key genes to ascertain the significant pathways.

Cell culture, plasmid construction, and generation of stable cell lines

The RCC cell lines 769-P and Caki-1 were obtained from the American Type Culture Collection (ATCC, Manassas, VA, USA) in October 2023. These cell lines were authenticated through short tandem repeat profiling to confirm their identity. Mycoplasma contamination was evaluated using PCR-based assays, and no contamination was detected. The most recent authentication and testing occurred in November 2023. The cells were cultured in Dulbecco's Modified Eagle's Medium supplemented with 10% fetal bovine serum, 1% penicillin-streptomycin, and 1% L-glutamine in a humidified atmosphere containing 5% CO_2 at 37 °C. The coding sequence for the human ATP1A1 protein was synthesized and cloned into the lentiviral vector pLVX. Concurrently, shRNA sequences targeting the ATP1A1 gene were designed using an online tool and subsequently cloned into the lentiviral vector pLKO.1. Lentiviral particles were produced in 293T cells and used to infect the 769-P and Caki-1 cell lines. At 72 h post-infection, selection was performed using puromycin at a final concentration of 8 μg/mL, followed by continuous culture for 7 days to establish stable cell lines.

Cellular proliferation

The cells were seeded into 96-well plates at a density of 2×10^4 cells per well. Cell proliferation was assessed using a CCK-8 kit (DOJINDO, Japan) and an EdU assay (Cell-Light™ EdU Apollo®594, UE, China), in accordance with the protocols provided by the respective manufacturers. In the CCK-8 assay, absorbance was measured at 450 nm using a microplate reader (Tecan, Switzerland). EdU-positive cells were visualized with a fluorescence microscope (Nikon, Japan), and the percentages of EdU-positive cells were quantified using ImageJ software.

Apoptosis analysis

Flow cytometry was utilized to evaluate apoptosis following the manufacturer's protocols. Briefly, treated cells were harvested after digestion with 0.25% trypsin (Gibco, USA) and washed twice with cold phosphate-buffered saline (PBS). The cells were then resuspended in 500 μl of binding buffer, to which 5 μl of Annexin V-FITC and 5 μl of propidium iodide (PI) solution were added. This mixture was incubated for 15 min at room temperature in the dark. Finally, the levels of apoptosis were analyzed using flow cytometry (CytoFLEX, Beckman Coulter, USA).

Glycolysis pressure test

The extracellular acidification rate (ECAR), a key metabolic indicator, was employed to evaluate glycolytic flux using the Seahorse XFP Extracellular Flux Analyzer (Agilent, USA), in accordance with the manufacturer's instructions. Treated ccRCC cells were uniformly distributed onto a 24-well XF cell culture plate (Seahorse Bioscience, USA) at a density of 5×10^4 cells per well. Following an overnight incubation to facilitate cell adhesion, the culture medium was replaced with fresh medium containing the specified assay reagents. The cartridge was subsequently loaded with glucose (10 mM), oligomycin (1 μM), and 2-deoxyglucose (2-DG, 50 mM) to measure ECAR at predetermined time intervals.

Mitochondrial stress test

Mitochondrial function was assessed by directly measuring the oxygen consumption rate (OCR) using a Seahorse XFP Extracellular Flux Analyzer (Agilent, USA) in accordance with the manufacturer's guidelines. Briefly, treated cells were seeded in 6-well plates and incubated for 24 h. Subsequently, the culture medium was replaced with Seahorse buffer, and automatic injections of oligomycin (1 μmol/L), FCCP (0.5 μmol/L), and rotenone/antimycin A (0.5 μmol/L) were administered. Following the

injections, OCR values were recorded, normalized to total protein content, and presented as mean ± SD.

Lactate production assay

Extracellular lactate levels were quantified using an L-Lactate Assay Kit (Beyotime, China) in accordance with the manufacturer's instructions. Briefly, cells were plated in 96-well plates at a density of 1×10^4 cells per well and incubated for 24 h. The culture supernatants were then collected and treated with a reaction buffer containing WST-8 at 37 °C for 30 min. Absorbance was measured at 450 nm using a microplate reader (Tecan, Switzerland). Lactate concentrations were determined from a standard curve and normalized to the total cell counts.

ATP quantification

Intracellular ATP levels were measured using an ATP Assay Kit (MedChemExpress, China). Cells were lysed in ATP lysis buffer, and the lysates were centrifuged at $12{,}000 \times g$ for 5 min at 4 °C. The resulting supernatants were combined with the ATP detection working solution, and luminescence was measured immediately using a microplate reader (Tecan, Switzerland). ATP concentrations were quantified against an ATP standard curve and normalized to the protein concentration of each sample.

Western blot (WB) analysis

Tissues and cells were lysed using ice-cold RIPA buffer supplemented with a protease inhibitor cocktail (Merck, USA). Protein concentrations were accurately determined using a BCA Protein Assay (Cwbio, China). Following protein extraction and quantification, proteins were separated by 10% SDS-PAGE (sodium dodecyl sulfate–polyacrylamide gel electrophoresis) (Bio-Rad, USA) and subsequently transferred onto nitrocellulose membranes (Millipore, USA). To block non-specific binding sites, the membranes were incubated in 5% non-fat milk for 40 min. The membranes were then exposed to primary antibodies at 4 °C overnight to ensure optimal and specific binding of target proteins. Subsequently, IR Dye-conjugated secondary antibodies were used to incubate the membranes for 1 h at room temperature. Bands were visualized using an Odyssey imaging system (LI-COR, USA). Densitometric analysis of the blots was conducted using ImageJ software. All primary and secondary antibodies utilized in this study, along with their supplier information, are listed in Supplementary Table S1.

Mitochondrial ROS detection

Mitochondrial ROS levels were evaluated using the MitoSOX™ Red mitochondrial superoxide indicator (Beyotime, China). Cells cultured on glass coverslips were treated with 5 μM MitoSOX™ reagent diluted in serum-free medium at 37 °C for 30 min in the dark. Following this, the cells were washed with PBS, and the nuclei were counterstained with DAPI. Fluorescence images were acquired using a laser confocal microscope (Leica TCS SP8, Germany) at excitation and emission wavelengths of 510 nm and 580 nm, respectively.

Molecular docking and visualization

The structural interaction between *ATP1A1* (UniProt ID: P05023) and SRC (UniProt ID: P12931) was predicted through molecular docking simulations. The three-dimensional coordinates of *ATP1A1* and SRC were derived from models predicted by AlphaFold3, which provide high-confidence structural predictions based on primary amino acid sequences. Prior to docking, the structures were optimized by adding polar hydrogens and assigning Gasteiger charges using PyMOL (v2.5.2). This step ensures accurate handling of electrostatic interactions during the docking process. The top-ranked conformation, exhibiting the lowest binding energy, was selected for visualization in PyMOL (v2.5.2). Hydrogen bonds and hydrophobic interactions were analyzed using the "Measurement" tool and visualized with PyMOL's "Publication" presets, focusing on distances and angles characteristic of key non-covalent interactions, such as hydrogen bonds (≤3.5 Å) and hydrophobic contacts.

Co-immunoprecipitation (Co-IP)

Endogenous interactions between *ATP1A1* and SRC were validated through Co-IP assays using lysates derived from 769-P and Caki-1 cell lines. Cells were co-transfected with plasmids that overexpressed *ATP1A1* and SRC, followed by lysis in an immunoprecipitation (IP) buffer consisting of 50 mM Tris-HCl (pH 7.4), 150 mM NaCl, 1% NP-40, and 5 mM EDTA, with additional protease and phosphatase inhibitors. To reduce non-specific binding, the lysates were pre-cleared using Protein A/G magnetic beads for 1 h at 4 °C. For each reaction, 500 μl of lysate was incubated overnight at 4 °C with 2 μg of either anti-*ATP1A1* or anti-SRC antibodies, followed by a 2-h incubation with Protein A/G magnetic beads. The magnetic beads were washed three times with IP buffer, and the bound proteins were eluted in 2×SDS-PAGE loading buffer and heated at 95 °C for 5 min. The eluates were then resolved by SDS-PAGE (10%) and subjected to immunoblotting with the specified antibodies. As a negative control, the same experimental procedure was performed using isotype-matched IgG antibodies instead of the primary antibodies. Input samples, representing the total cell lysate, served as a positive control.

Tumorigenesis assay

The experimental procedures involving animals complied with the guidelines established by the Animal Ethics Committee of the Institute of Medical Biology, Chinese Academy of Medical Sciences. Female BALB/c nude mice, aged 4–5 weeks and weighing between 18 and 20 g, were obtained from Charles River Laboratories (Beijing, China). The mice were housed in a specific pathogen-free facility with controlled environmental conditions, including humidity levels maintained between 40% and 60% and temperatures kept between 18 °C and 23 °C. They were provided with a standard rodent diet and had ad libitum access to filtered water. To establish the experimental model, the mice were injected with 1×10^6 769-P cells expressing *ATP1A1* or an empty vector ($n = 4$ per group). Approximately 7 days post-injection, tumor growth was monitored by measuring both tumor length (longest dimension, L) and width (shortest dimension, W) every 3 days over a period of 4 weeks. For treatments involving pNaktide, BALB/c nude mice ($n = 5$ per group, randomly allocated) that had been subcutaneously injected with 1×10^6 769-P cells were subsequently administered saline or pNaktide (at doses of 10 and 25 mg/kg body weight) every other day for a total of five treatments. Tumor volumes were calculated using the formula: $V = 1/2\ (L \times W^2)$. The endpoint of each experiment was determined to ensure that the tumor length did not exceed 1.5 cm in the group exhibiting the fastest tumor growth. Primary tumors were harvested for further studies.

Immunohistochemistry (IHC) and immunofluorescence (IF) assays

Paraffin-embedded samples were serially sectioned to a thickness of 4 μm. Antigen retrieval achieved was through microwave irradiation for 30 min in a 0.01 M citrate buffer (pH 6.0), followed by a 5-min treatment with 3% hydrogen peroxide. The sections were incubated overnight at 4 °C with primary antibodies. Subsequently, the tissues were incubated with secondary antibodies for 1 h at room temperature and stained with diaminobenzidine until brown granules became visible. For immunofluorescence assays, cells cultivated in 24-well plates were fixed with 4% paraformaldehyde (w/v) and incubated overnight at 4 °C with primary antibodies. The cells were then exposed to fluorophore-conjugated secondary antibodies (all antibodies are detailed in Supplementary Table S1). Nuclei were stained with DAPI, and the slides were examined using a laser confocal microscope (Leica TCS SP8, Germany).

Statistical analysis

Statistical analyses were performed using Student's *t*-test to compare two groups and one-way ANOVA for comparisons among multiple groups. These analyses were conducted with GraphPad Prism 9.0, and differences between groups were considered statistically significant at three levels: $^*P < 0.05$, $^{**}P < 0.01$, and $^{***}P < 0.001$.

RESULTS

Downregulated expression of *ATP1A1* in ccRCC is associated with poor prognosis

We first utilized the UALCAN data portal to analyze *ATP1A1* expression in the TCGA ccRCC dataset. The analysis demonstrated that *ATP1A1* mRNA expression was significantly reduced in primary tumors compared to normal tissues (Fig. 1A). This reduction was consistent across all cancer grades (G1, G2, G3, and G4) (Fig. 1B) and pathological stages (S1, S2, S3, and S4) (Fig. 1C). Additionally, analysis of the ccRCC dataset revealed that

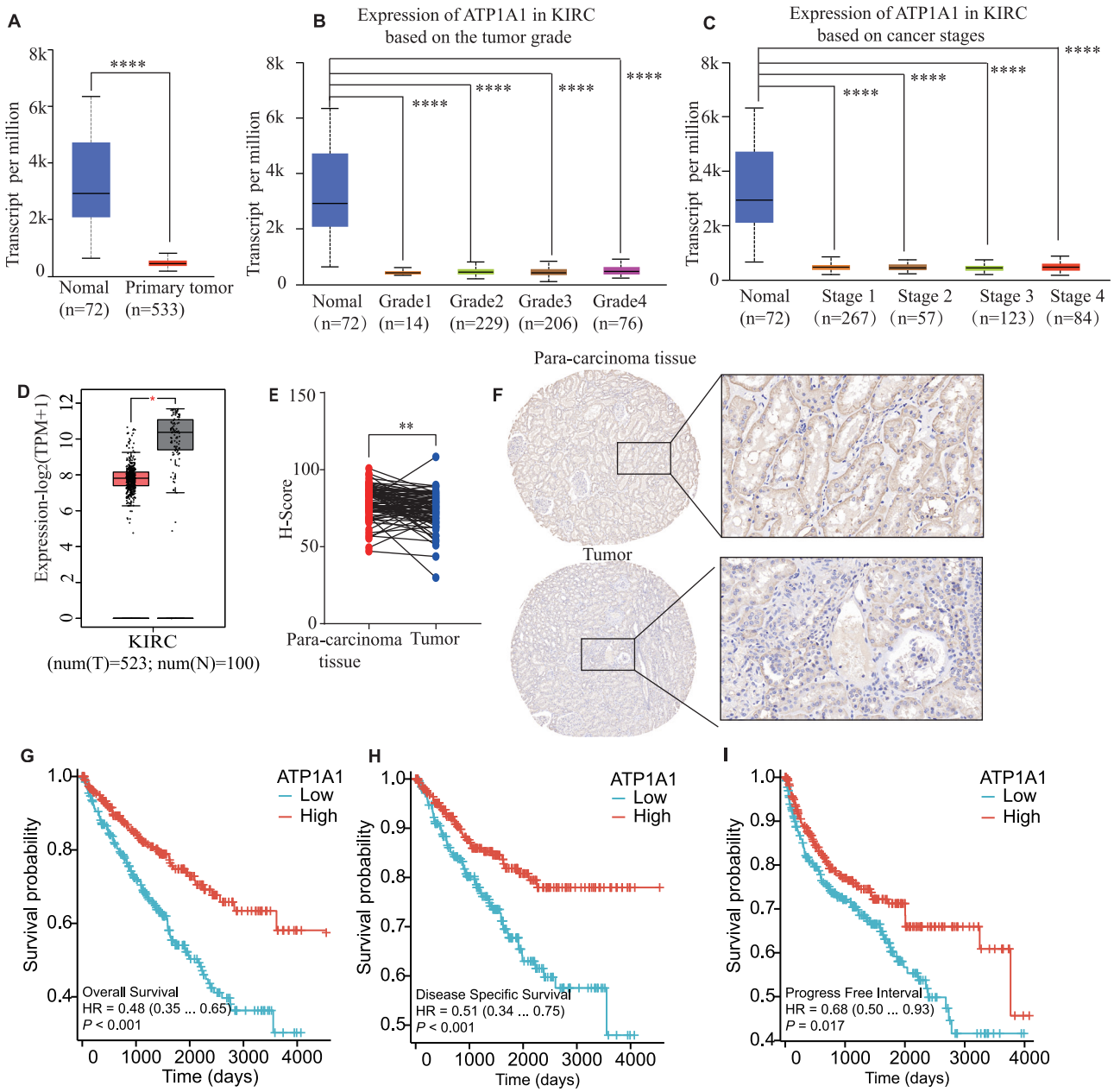

Fig. 1 *ATP1A1* is significantly downregulated in ccRCC and is positively correlated with prognosis. A Box-whisker plots depict the expression levels of *ATP1A1* in tumor tissues compared to normal tissues, according to the *t*-test in TCGA by UALCAN. Box-whisker plots display the *ATP1A1* transcription in subgroups of patients with CRCC, stratified based on tumor grades (**B**) and individual cancer stage (**C**). **D** A Box-whisker plot presents the expression levels of *ATP1A1* in tumor tissues and normal tissues, according to the *t*-test in TCGA using GEPIA2. **E** A statistical analysis of *ATP1A1* immunostaining score in clinical samples ($n = 70$). **F** Representative images for *ATP1A1* protein levels, as shown by IHC immunoassay. OS (**G**), DSS (**H**), and DFI (**I**) of *ATP1A1* in TCGA ccRCC cohort analysis from Kaplan–Meier survival curves. *$P < 0.05$; **$P < 0.01$; ***$P < 0.001$; ****$P < 0.0001$.

ATP1A1 protein expression was also significantly decreased in tumors relative to normal tissues (Fig. 1D), corroborating the mRNA expression findings. Furthermore, we conducted IHC analysis of tissue microarrays containing tumors and paired adjacent non-tumor tissues from 70 ccRCC patients. The immunostaining scores indicated reduced *ATP1A1* expression in tumor tissues compared to adjacent non-tumor tissues (Fig. 1E, F). Moreover, Kaplan–Meier survival analysis based on TCGA data demonstrated that low *ATP1A1* expression correlated with shorter OS (Fig. 1G), DSS (Fig. 1H), and PFI (Fig. 1I) in ccRCC patients. These findings suggest that low *ATP1A1* expression is an independent risk factor for poor prognosis in ccRCC and may serve as a valuable prognostic marker warranting further clinical validation.

ATP1A1 inhibits the proliferation of ccRCC both in vitro and in vivo

In this study, we aimed to elucidate the role of *ATP1A1* in the growth of ccRCC cells. We commenced by evaluating the expression levels of RCC cell lines, specifically ACNH, 769-P, 786-O, and Caki-1, utilizing Western blotting. Our analysis revealed that *ATP1A1* expression was significantly lower in the 769-P and Caki-1 cell lines (Fig. 2A). Immunofluorescence (IF) analysis indicated that

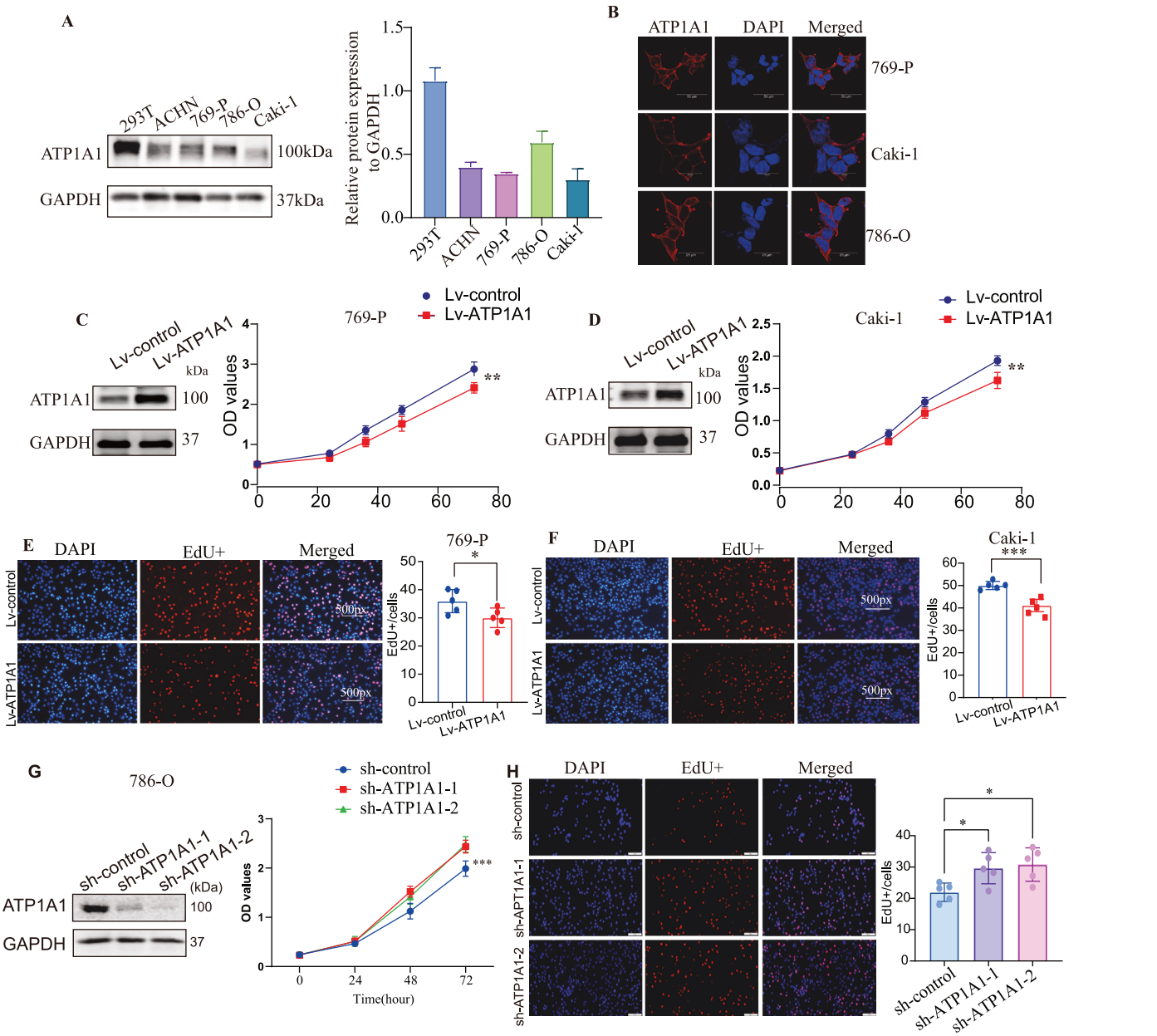

Fig. 2 ***ATP1A1* inhibits the proliferation of ccRCC in vitro. A** The expression of *ATP1A1* across various ccRCC cell lines was assessed by WB. Quantification was based on three independent biological replicates ($n = 3$). **B** Immunofluorescence microscopy revealed a perinuclear and potentially membrane-associated distribution pattern of *ATP1A1* in ccRCC cell lines. The proliferation of 769-P cells (**C**) and Caki-1 cells (**D**) was evaluated in response to *ATP1A1* overexpression using the CCK-8 assay, with data analyzed via repeated measures ANOVA ($n = 5$). The impact of *ATP1A1* on the growth of 769-P cells (**E**) and Caki-1 cells (**F**) was further investigated through the EdU assay following *ATP1A1* overexpression, with results also analyzed using repeated measures ANOVA ($n = 5$). Quantitative analysis results are presented. **G** The proliferation of 786-O cells was evaluated in response to *ATP1A1* knockdown using the CCK-8 assay, with data analyzed via repeated measures ANOVA ($n = 5$). **H** The impact of *ATP1A1* on the growth of 786-O was further investigated through the EdU assay following *ATP1A1* knockdown, with results also analyzed using repeated measures ANOVA ($n = 5$). Quantitative analysis results are presented. $^{*}P < 0.05$; $^{**}P < 0.01$; $^{***}P < 0.001$; $^{****}P < 0.0001$.

ATP1A1 exhibited a perinuclear and potentially membrane-associated distribution in ccRCC cells (Fig. 2B). Subsequently, we established *ATP1A1* overexpression cell lines (769-P and Caki-1) and *ATP1A1*-knockdown cell lines (786-O) to assess their proliferation via the CCK-8 assay. The results revealed that the overexpression of ATP1A1 significantly inhibited the proliferation of both 769-P (Fig. 2C) and Caki-1 cells (Fig. 2D), while *ATP1A1* knockdown resulted in increased proliferation of 786-O cells (Fig. 2G). Additionally, EdU assays corroborated these findings, revealing a decrease in EdU-positive cells in *ATP1A1*-overexpressing 769-P (Fig. 2E) and Caki-1 cells (Fig. 2F), alongside an increase in EdU-positive cells in *ATP1A1*-knockdown 786-O cells (Fig. 2H).

Furthermore, we investigated the potential influence of *ATP1A1* on tumor growth in vivo. Equal amounts of 769-P cells, which overexpress *ATP1A1*, were injected into nude mice, and tumor formation was closely monitored. The results demonstrated that the overexpression of *ATP1A1* in 769-P cells resulted in significantly reduced tumor volumes (Fig. 3A, B) and weights (Fig. 3C) in the nude mice compared to the control group. IHC analysis for Ki67 revealed a lower proportion of Ki67-positive cells

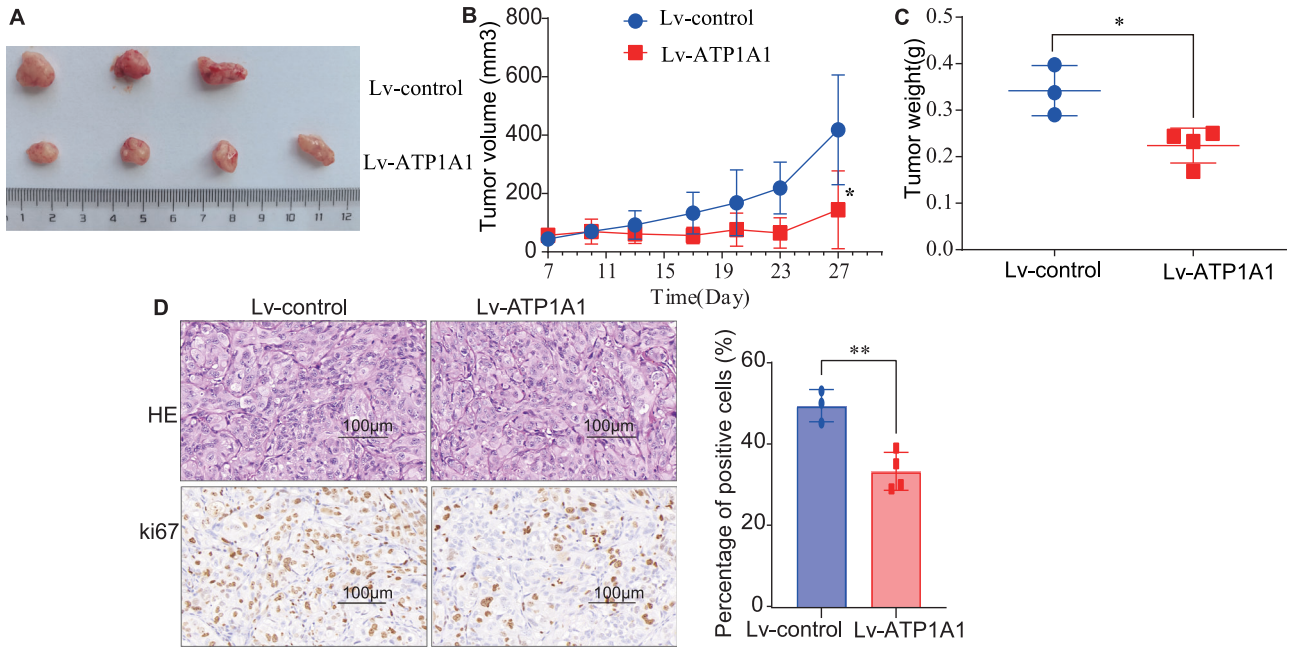

Fig. 3 *ATP1A1* inhibits the proliferation of ccRCC in vivo. A A representative image of tumor growth in nude mice subcutaneously inoculated with 769-P cells that overexpress *ATP1A1*. **B** The tumor-growth curve for nude mice that were subcutaneously injected with 769-P cells overexpressing *ATP1A1*, with tumor sizes measured every 3 days over a period of 4 weeks. **C** Tumor weights were collected from the post-sacrifice subcutaneous mouse model. **D** IHC analysis of Ki67 shows a decreased proportion of Ki67-positive cells in tumors derived from *ATP1A1*-overexpressing cells. *$P < 0.05$; **$P < 0.01$.

in the tumors of *ATP1A1*-overexpressing mice (Fig. 3D). These findings confirm that *ATP1A1* inhibits the proliferation of ccRCC cells both in vitro and in vivo.

Key pathway regulation of *ATP1A1* in ccRCC

To elucidate the biological significance of *ATP1A1* in ccRCC, we analyzed the ccRCC transcriptome dataset from the TCGA database, which comprises 613 tumor samples and 72 adjacent normal tissues. We filtered out genes with extremely low expression (Median TPM < 0.5), identifying 107 co-expressed genes. The heatmap presented in Fig. 4A displays the top 20 genes with the highest correlation coefficients. Subsequently, we utilized the STRING database and the cytoHubba plugin in Cytoscape to identify the top 10 hub genes, which include *CLDN7*, *MUC1*, *PPARGC1A*, *OCLN*, and *IRS1* (Fig. 4B). Further KEGG pathway analysis of these key regulatory genes revealed significant enrichment in metabolic diseases and pathways related to metabolism, such as oxidative phosphorylation and the TCA cycle (Fig. 4C). To gain deeper insights into the regulatory pathways, we conducted GO analysis. In biological processes (BP), these genes were significantly enriched in energy derivation through the oxidation of organic compounds, cellular respiration, and aerobic respiration (Fig. 4D). In terms of cellular components (CC), these genes were predominantly enriched in mitochondria, cytoplasm, and cell membranes (Fig. 4E), indicating their vital functions in specific cellular regions, particularly in energy metabolism and substance transport. Regarding molecular functions (MF), these genes were significantly enriched in phospholipid binding, primary active transmembrane transporter activity, and proton transmembrane transporter activity (Fig. 4F), emphasizing their critical roles in metabolic regulation and signal transduction. To further investigate the functional relevance of *ATP1A1*, we conducted a Pearson correlation analysis between *ATP1A1* and key regulators of oxidative phosphorylation. The results revealed significant moderate positive correlations between *ATP1A1* and *PPARGC1A* ($R = 0.540$, $P < 0.001$), *SIRT1* ($R = 0.553$, $P < 0.001$), and *AKT1* ($R = 0.598$, $P < 0.001$). Additionally, a weak correlation was observed with *HIF1A* ($R = 0.469$, $P < 0.001$) (Fig. 4G). Collectively, these findings suggest that *ATP1A1* may play a role in metabolic reprogramming in ccRCC by modulating the molecular networks associated with the oxidative phosphorylation pathway.

ATP1A1 induces metabolic reprogramming via suppressing SRC/ERK signaling to promote apoptosis in ccRCC

To investigate whether the observed growth suppression induced by *ATP1A1* overexpression was associated with the reprogramming of energy metabolism, we assessed the effects on OXPHOS and glycolysis using the Seahorse XF assay, a standard method for measuring key parameters of cellular metabolism. Our results demonstrated that *ATP1A1* overexpression in 769-P and Caki-1 cells significantly enhanced OXPHOS, as evidenced by increased ATP production, maximal respiration, and spare respiratory capacity (Fig. 5A, B), while simultaneously reducing glycolytic capacity and reserve (Fig. 5C, D). Furthermore, flow cytometry analysis revealed an increase in apoptosis among *ATP1A1*-overexpressing cells (Fig. 5E, F). Given that OXPHOS is a critical source of ROS production, we employed the mitochondria-specific superoxide probe MitoSO™ Red to detect intracellular ROS activity. The results showed a significant increase in the red fluorescence signal in 769-P and Caki-1 cells overexpressing *ATP1A1*, indicating elevated mitochondrial ROS levels (Fig. 5G).

To further validate the metabolic reprogramming induced by *ATP1A1* overexpression, we conducted additional assays to quantify intracellular ATP and extracellular lactate levels. As illustrated in Supplementary Fig. S1A, the overexpression of *ATP1A1* significantly increased intracellular ATP levels while concurrently reducing extracellular lactate production in both Caki-1 and 769-P cells. This finding further supports enhanced OXPHOS and a reduction in glycolysis. These results reinforce the hypothesis that *ATP1A1* promotes a metabolic shift toward mitochondrial respiration, thereby increasing ROS production and apoptosis in ccRCC cells.

Previous studies have reported that *ATP1A1* interacts with SRC across various tumors. Our analysis of clinical data from the TCGA database for ccRCC indicated a significant increase in SRC

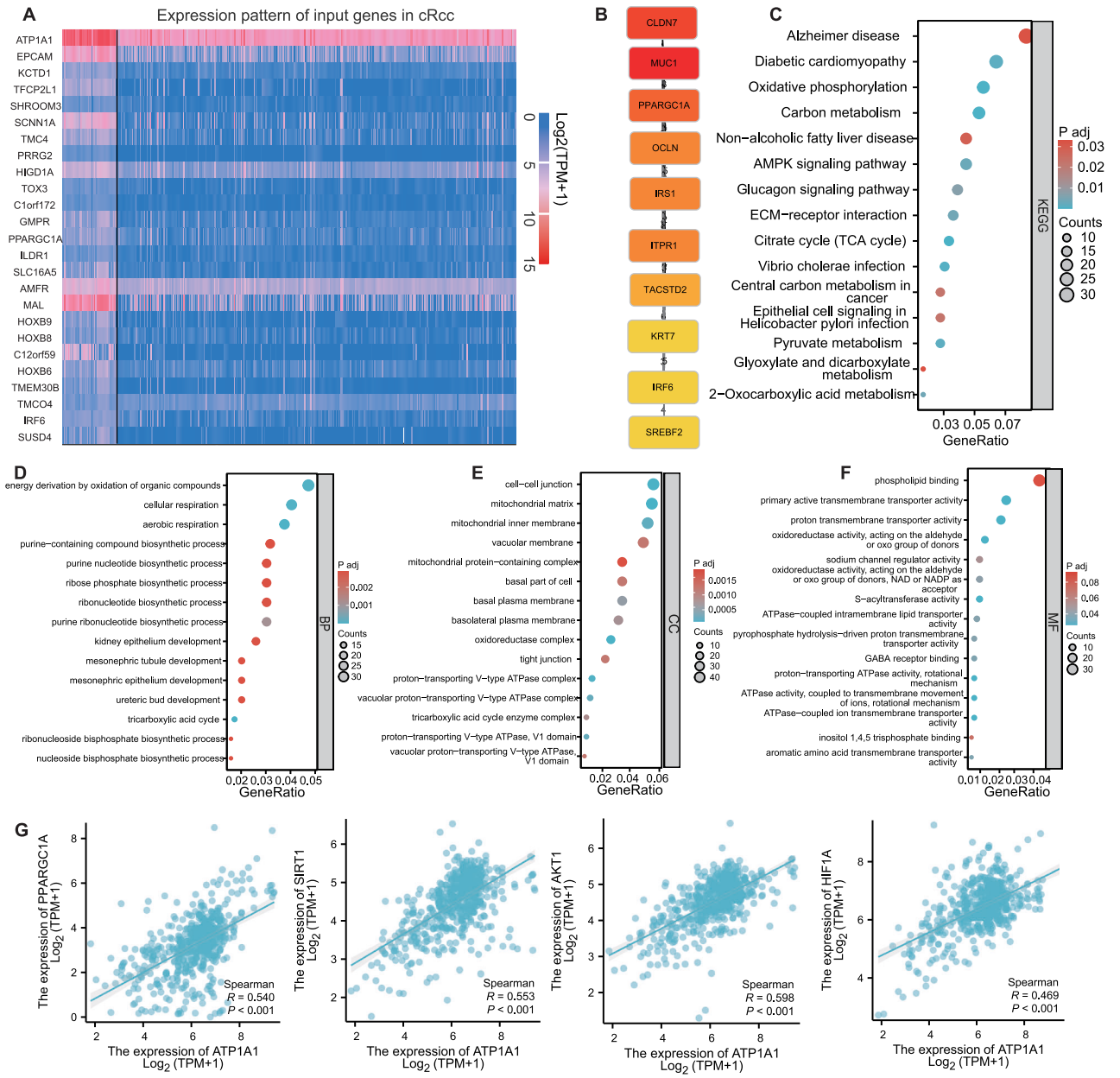

Fig. 4 Analysis of *ATP1A1* co-expressed genes and pathways in ccRCC. A A heatmap showing the top 20 *ATP1A1*-related genes identified in ccRCC. **B** The top 10 hub genes among the *ATP1A1* co-expressed genes in ccRCC, as analyzed by cystoscope, were displayed. **C** The KEGG enrichment analysis for *ATP1A1* co-expressed genes was shown. **D**–**F** The GO enrichment analysis across the categories of Biological Process (BP), Cellular Component (CC), and Molecular Function (MF) for *ATP1A1* co-expressed genes. **G** Scatter plots depicting Spearman correlations between *ATP1A1* mRNA expression and key phospho-regulators (*PPARGC1A, SIRT1, AKT1, HIF1A*) in the TCGA ccRCC cohort ($n = 613$ tumors). The absolute value of the correlation coefficient (R) represents the strength of the correlation: 0–0.3 indicates weak or no correlation; 0.3–0.5 indicates a weak correlation; 0.5–0.8 indicates a moderate correlation; 0.8–1 indicates a strong correlation. Statistical significance is determined by p values, with $p < 0.05$ indicating a significant difference.

expression in tumor tissues compared to normal tissues (Fig. 5H). In ccRCC cell lines overexpressing *ATP1A1*, we observed a decrease in the phosphorylation of SRC and ERK, accompanied by an upregulation of cytochrome c (cyto C) and cleaved caspase 9 (Fig. 5I). These findings suggest that *ATP1A1* may induce a metabolic switch to mitochondrial respiration, leading to increased ROS production and promoting apoptosis in ccRCC. This highlights the potential of *ATP1A1* as a therapeutic target in ccRCC.

To further investigate the molecular interactions between *ATP1A1* and SRC, we employed AlphaFold3 for structural predictions and utilized PyMOL for three-dimensional conformational analyses of both proteins. The results revealed a significant spatial proximity between key amino acid residues of *ATP1A1* and SRC, with a measured Cα–Cα distance of 2.9 Å (Fig. 5J). This distance falls within the optimal range for hydrogen bond donor-acceptor interactions (2.6–3.2 Å), strongly suggesting the presence of critical charge-dipole interactions. To validate these structural predictions, co-localization experiments in the 769-P and Caki-1 cell lines demonstrated substantial spatial overlap in the intracellular distribution of *ATP1A1* and SRC, providing visual support for the likelihood of direct interaction (Fig. 5K). Additionally, Co-IP assays conducted in these cell lines confirmed the in vivo formation of *ATP1A1*-SRC protein complexes (Fig. 5L). Collectively, these findings indicate

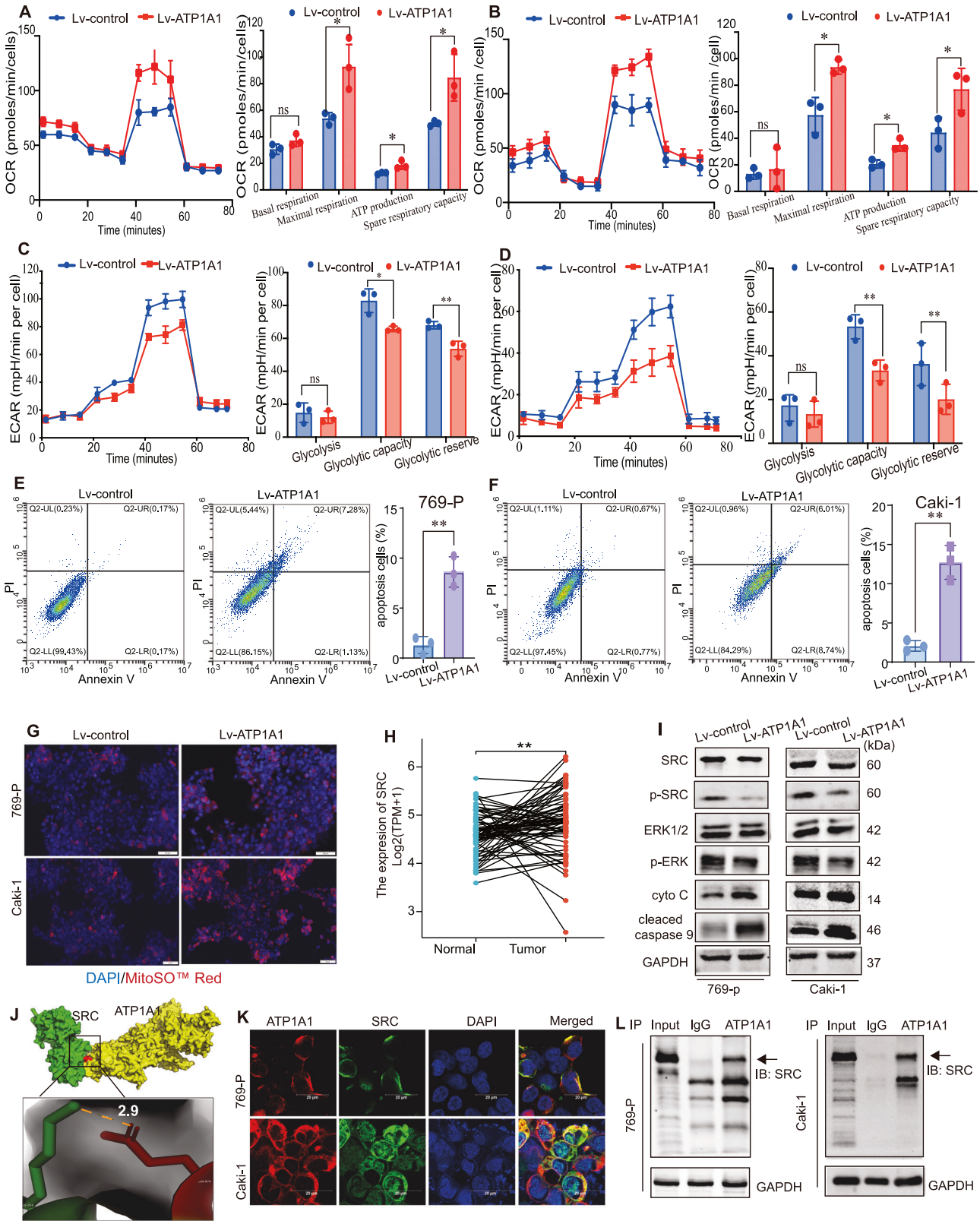

that *ATP1A1* promotes apoptosis through mitochondrial pathways by directly binding to SRC, inhibiting its phosphorylation, and subsequently downregulating the ERK signaling pathway. These results underscore the therapeutic potential of targeting *ATP1A1* as a molecular intervention strategy in ccRCC.

Reactivation of SRC reverses the antitumor effects of *ATP1A1*

To determine whether SRC inhibition is essential for *ATP1A1*-mediated suppression of tumor cell phenotypes, we first examined SRC phosphorylation levels following *ATP1A1* knockdown. In 786-O cells, silencing *ATP1A1* resulted in a significant

Fig. 5 *ATP1A1* overexpression promotes apoptosis in ccRCC via ROS and SRC/ERK pathway. The OXPHOS levels, including ATP production, maximal respiration, and spare respiratory capacity in 769-P (**A**) and Caki-1 (**B**) cells overexpressing *ATP1A1*, were evaluated using Seahorse XF. The glycolytic capacity and reserve in 769-P (**C**) and Caki-1(**D**) cells with *ATP1A1* overexpression were analyzed by Seahorse XF. The apoptosis rates in 769-P (**E**) and Caki-1 (**F**) overexpressing *ATP1A1* were analyzed by flow cytometry. **G** The intracellular ROS levels in *ATP1A1*-overexpressing cells were detected by the mitochondria-targeted superoxide probe MitoSOᵀᴹ Red. **H** The SRC expression in ccRCC tumor tissues compared to normal tissues was analyzed by the TCGA database. **I** The levels of SRC, p-SRC, ERK1/2, p-ERK1/2, cyto c, and cleaved caspase 9 in 769-P and Caki-1 cells overexpressing *ATP1A1* were detected by WB. **J** Predicted 3D conformation of *ATP1A1* (yellow) and SRC (green) generated by AlphaFold3, with PyMol visualization showing spatial proximity between *ATP1A1* and SRC. Dashed line indicates Cα–Cα distance (2.9 Å), within hydrogen bonding range (2.6–3.2 Å). **K** Representative immunofluorescence images showing the subcellular localization of *ATP1A1* (red) and SRC (green) in 769-P and Caki-1 cells. **L** Co-IP method to detect the interaction between *ATP1A1* and SRC in 769-P and Caki-1 cells. *$P < 0.05$; **$P < 0.01$.

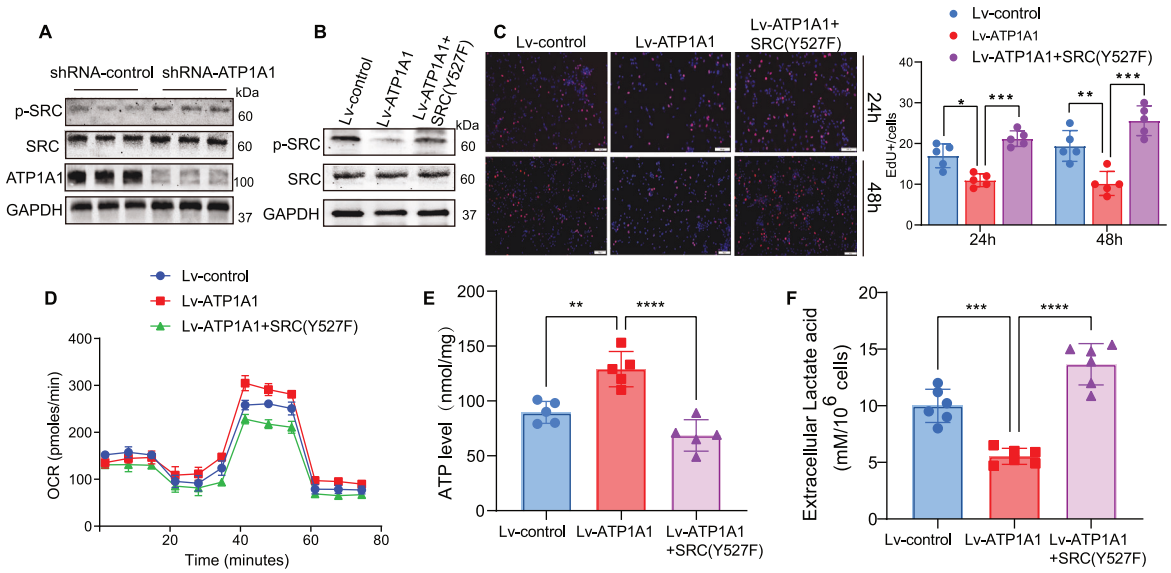

Fig. 6 Reactivation of SRC reverses the inhibitory effects of *ATP1A1* overexpression. A Western blot analysis showing increased phosphorylation of SRC following *ATP1A1* knockdown in 786-O cells. **B** Western blot confirming successful reactivation of SRC signaling in *ATP1A1*-overexpressing 769-P cells transfected with a constitutively active SRC mutant (Y527F). **C** EdU incorporation assay showing that SRC reactivation partially restored the proliferation of *ATP1A1*-overexpressing cells. OCR (**D**) and intracellular *ATP* levels (**E**) were reduced, while extracellular lactate production (**F**) was increased in *ATP1A1*-overexpressing cells; these metabolic alterations were reversed upon SRC reactivation. *$P < 0.05$; **$P < 0.01$; ***$P < 0.001$; ****$P < 0.0001$.

increase in phosphorylated SRC, indicating that *ATP1A1* negatively regulates SRC activation (Fig. 6A).

To further evaluate whether SRC reactivation could counteract the phenotypic effects induced by *ATP1A1* overexpression, we transfected 769-P cells, which stably overexpress ATP1A1 with a constitutively active SRC mutant (Y527F). The Y527F mutation disrupts the inhibitory phosphorylation site of SRC, thereby maintaining the kinase in a constitutively active state [23]. Western blot analysis confirmed the successful reactivation of SRC signaling in these cells (Fig. 6B). Functionally, SRC reactivation significantly reversed the *ATP1A1*-induced suppression of cell proliferation, as demonstrated by increased EdU incorporation (Fig. 6C). Additionally, *ATP1A1* overexpression reduced the OCR, decreased intracellular ATP levels, and increased extracellular lactate production—all of which were significantly restored upon SRC reactivation (Fig. 6E, F).

Together, these results indicate that the antitumor effects of *ATP1A1* are, at least in part, mediated through the suppression of SRC signaling.

pNaktide significantly inhibits the proliferation of ccRCC and promotes a metabolic shift by suppressing the SRC pathway

To evaluate whether pNaktide can serve as a substitute for exogenous *ATP1A1* in its suppressive role, 769-P and Caki-1 cells were treated with pNaktide at concentrations of 1, 2, 5, and 10 μM for 48 h. The results indicated that treatment with 10 μM pNaktide significantly altered the energy metabolism of 769-P cells, specifically resulting in a reduction in glycolytic capacity and glycolytic reserve (Fig. 7A), along with a significant increase in ATP production, maximal respiration, and spare respiratory capacity (Fig. 7B). Flow cytometry was employed to further assess the effect of pNaktide on cell viability. The findings demonstrated that both 5 μM and 10 μM pNaktide significantly induced apoptosis in both 769-P (Fig. 7C) and Caki-1 cells (Fig. 7D). Furthermore, the production of ROS increased significantly with rising concentrations of pNaktide (Fig. 7E). Additionally, WB analysis revealed that pNaktide inhibited the phosphorylation levels of SRC and ERK while upregulating the expression levels of cyto C and cleaved caspase 9 (Fig. 7F). These findings suggest that pNaktide can substitute for exogenous *ATP1A1* by suppressing the SRC pathway, inhibiting glycolysis, accumulating elevated levels of ROS, and inducing apoptosis.

pNaktide as an exogenous *ATP1A1* additive restores inhibition of the SRC pathway in ccRCC

Our research confirms the significant inhibitory effects of pNaktide on the progression of ccRCC. We propose that pNaktide could be developed as a therapeutic agent targeting *ATP1A1* to correct SRC pathway abnormalities caused by *ATP1A1* down-regulation. Initially, we knocked down *ATP1A1* in 786-O cells and observed a substantial increase in phosphorylated SRC and ERK levels through WB analysis (Fig. 8A), demonstrating that

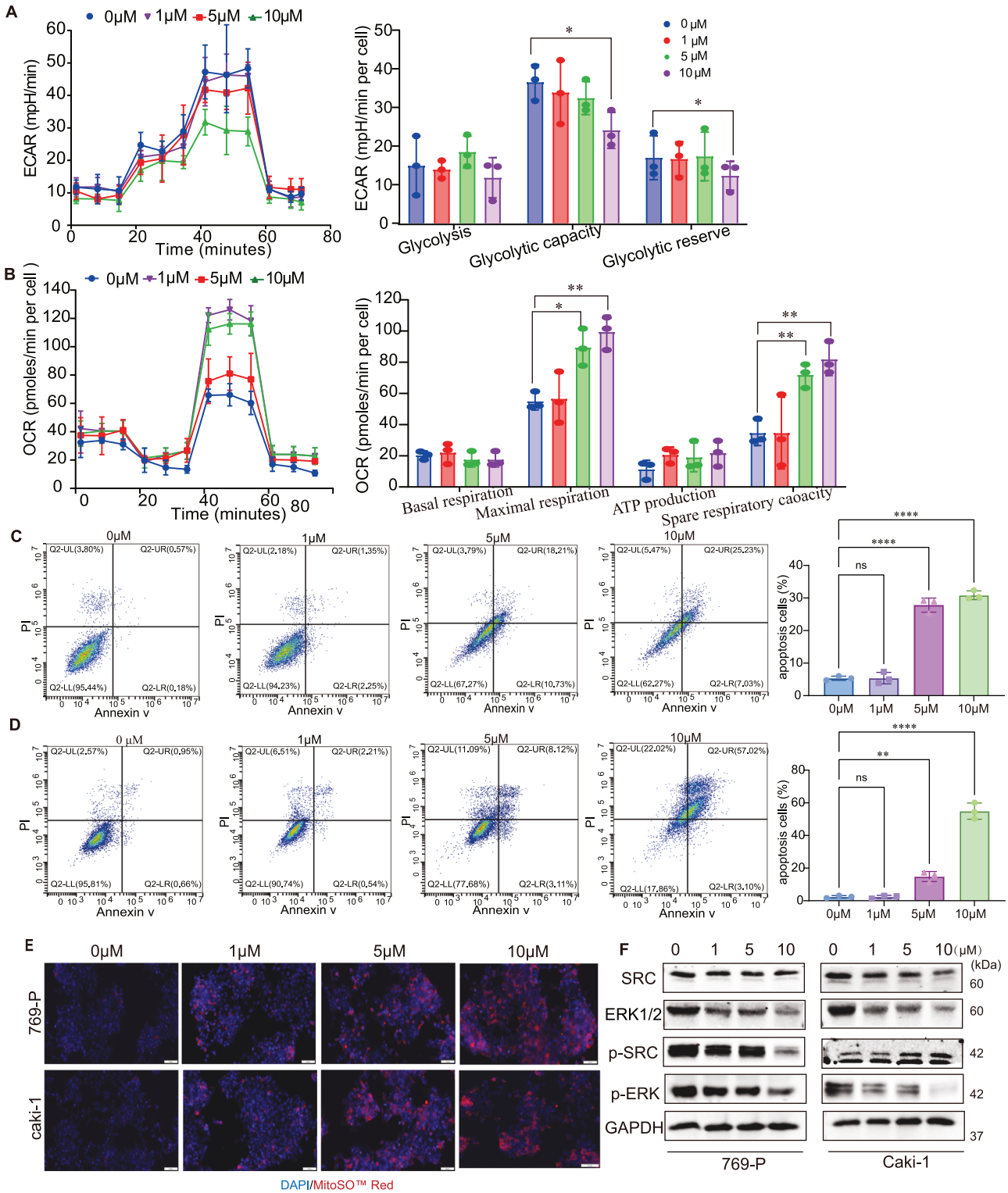

Fig. 7 pNaktide mimics the suppressive effects of exogenous *ATP1A1* in ccRCC cells. A The glycolytic capacity and reserve in 769-P cells treated with pNaktide were assessed using the Seahorse XF analyzer. **B** The OXPHOS levels, characterized by ATP production, maximal respiration, and spare respiratory capacity in 769-P cells treated with pNaktide, were detected by Seahorse XF. Apoptosis in 769-P (**C**) and Caki-1 cells (**D**) treated with pNaktide was analyzed by flow cytometry. **E** The intracellular ROS levels in 769-P and Caki-1 cells treated with varying concentrations of pNaktide were detected by the mitochondria-targeted superoxide probe MitoSO™ Red. **F** The levels of SRC, p-SRC, ERK1/2, p-ERK1/2, cyto c, and cleaved caspase 9 in 769-P and Caki-1 cells treated with pNaktide in a final concentration of 5 μM were detected by WB.

pNaktide can reverse the upregulation of SRC activity resulting from *ATP1A1* knockdown. Furthermore, CCK-8 proliferation assays indicated that *ATP1A1* knockdown markedly enhanced the proliferation capacity of 786-O cells; however, this enhanced proliferation was significantly suppressed by pNaktide treatment (Fig. 8B). Additionally, metabolic analyses revealed that pNaktide reversed the increased glycolytic capacity and promoted oxidative phosphorylation in *ATP1A1*-knockdown cells (Fig. 8C,

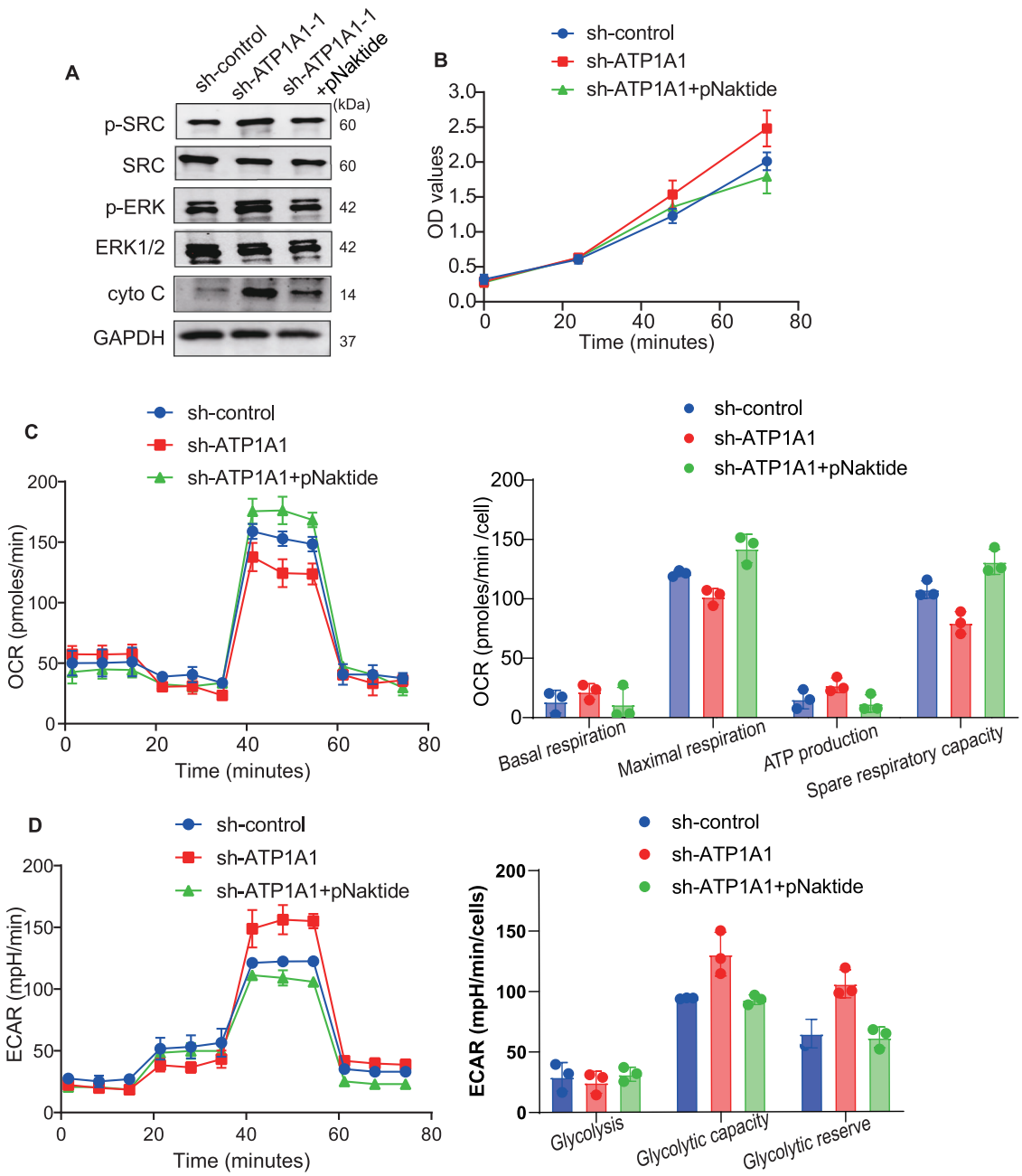

Fig. 8 pNaktide reverses SRC pathway activation and metabolic reprogramming induced by *ATP1A1* knockdown in ccRCC. A The levels of SRC, p-SRC, ERK1/2, p-ERK1/2, and cyto c in *ATP1A1*-knockdown 786-O cells, and then treated with pNaktide in a final concentration of 5 μM, were detected by WB. **B** The proliferative ability of 786-O cells with *ATP1A1* knockdown, following treatment with pNaktide, was evaluated by the CCK-8 method. **C** The OXPHOS levels, characterized by ATP production, maximal respiration, and spare respiratory capacity in 786-O with *ATP1A1* knockdown and treated with pNaktide, were detected by Seahorse XF. **D** The glycolytic capacity and reserve in 786-O cells subjected to *ATP1A1* knockdown and treated with pNaktide were detected by Seahorse XF. **P* < 0.05; ***P* < 0.01; ****P* < 0.001; *****P* < 0.0001.

D). In conclusion, pNaktide effectively modulates the SRC signaling pathway, reversing metabolic reprogramming and SRC pathway abnormalities associated with low *ATP1A1* expression in ccRCC.

pNaktide could inhibit the growth of xenograft tumors

To further investigate the potential of pNaktide as a therapeutic agent for ccRCC, we established a xenograft tumor model to evaluate its effects on ccRCC proliferation in vivo. Four to five-week-old nude mice were inoculated with 10^6 769-P cells and divided into three groups. The experimental groups received intraperitoneal injections of pNaktide at doses of 10 mg/kg and 25 mg/kg every 3 days, while the control group was administered PBS. Tumor volume and weight were significantly reduced in pNaktide-treated mice, particularly in the 25 mg/kg group (Fig. 9A, B). Immunohistochemical analysis for Ki67 revealed a substantial decrease in Ki67-positive cells in tumors from pNaktide-treated mice (Fig. 9C). WB analysis of tumor lysates demonstrated that pNaktide significantly inhibited SRC activity (Fig. 9D). These in vivo findings support the inhibitory effects of pNaktide on ccRCC progression observed in vitro. This research introduces a promising therapeutic strategy, suggesting that pNaktide, as an exogenous *ATP1A1* additive, has the potential to alter tumor cell metabolism and inhibit cancer progression.

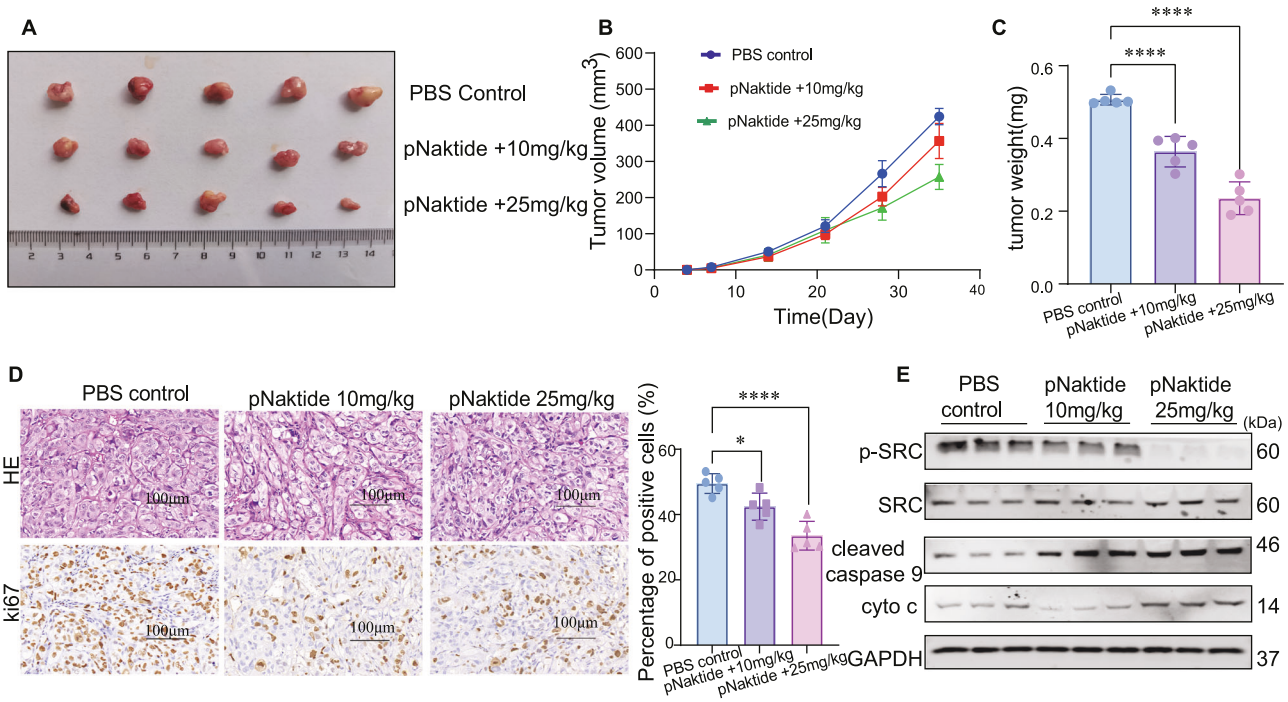

Fig. 9 pNaktide inhibits ccRCC tumor growth in vivo. A A representative image depicting tumor growth in a 769-P cell-derived xenograft model treated with pNaktide. **B** The tumor growth curve for nude mice was subcutaneously injected with 769-P cells and treated with pNaktide. **C** The tumor weight in the 769-P cell-derived xenograft model following treatment with pNaktide. **D** The Ki67-positive cells in tumors from pNaktide-treated mice were detected using IHC. **E** The levels of SRC, p-SRC, cyto c, and cleaved caspase 9 in the 769-P cell-derived xenograft model treated with pNaktide were detected by WB. $^{*}P < 0.05$; $^{**}P < 0.01$; $^{***}P < 0.001$; $^{****}P < 0.0001$.

DISCUSSION

Our research demonstrates that in ccRCC, *ATP1A1* interacts with SRC to regulate downstream signaling cascades, thereby influencing ccRCC cell metabolism to promote apoptosis and inhibit cell proliferation. However, we observed that the expression of *ATP1A1* is significantly downregulated in ccRCC tissues, while SRC expression is markedly upregulated. Notably, the addition of pNaktide can rectify the dysregulation of the SRC signaling cascade caused by the low expression of *ATP1A1*, significantly inhibiting the progression of ccRCC. Consequently, pNaktide emerges as a promising candidate for the development of novel therapeutic agents targeting ccRCC.

Recent studies have revealed that *ATP1A1* expression varies significantly across different tumor types and plays a crucial role in tumor progression. For instance, *ATP1A1* expression has been closely associated with tumor growth and patient prognosis in hepatocellular carcinoma [24], triple-negative breast cancer [13], colorectal cancer [12, 25], gastric cancer [11], and melanoma [8]. Moreover, certain compounds, such as Cynsaccatol L [5], Panax notoginseng [26], and Resibufogenin [27], have been demonstrated to target *ATP1A1*, thereby inhibiting tumor growth. In some cancers, the overexpression of *ATP1A1* is associated with increased invasiveness and poorer survival rates [11, 12, 24, 28], while in others, its low expression is linked to tumor suppression [10, 14]. These findings suggest that *ATP1A1* may exhibit distinct biological functions and clinical implications across various cancer types.

In RCC, *ATP1A1* has been reported to be significantly downregulated and associated with poor patient prognosis. RCC patients who are positive for *ATP1A1* exhibit a longer OS time compared to those who are *ATP1A1*-negative. Furthermore, the exogenous expression of *ATP1A1* has been shown to inhibit RCC cell proliferation and migration, as well as induce apoptosis by increasing ROS production [14]. Elevated levels of PGR/MC1 and the downregulation of *ATP1A1* both contribute to the activation of AKT phosphorylation, which enhances RCC cell growth and migration [29]. Our study found that *ATP1A1* is significantly downregulated in ccRCC and is closely associated with patient prognosis. Further research indicates that the overexpression of *ATP1A1* can inhibit the proliferation of ccRCC by altering cellular metabolism and promoting apoptosis, suggesting that *ATP1A1* may serve as a potential therapeutic target for ccRCC.

Recent research highlights significant interactions between *ATP1A1* and SRC, a non-receptor tyrosine kinase, in various cellular processes, particularly in cancer. *ATP1A1* interacts with SRC to activate its tyrosine phosphorylation, thereby triggering downstream signaling pathways, including MAPK/ERK and PI3K/AKT [17]. These pathways are closely associated with multiple oncogenic cellular processes, including migration, adhesion, invasion, proliferation, and survival [30]. A study involving 523 patients with ccRCC demonstrated that higher levels of SRC and Akt mRNA expression were strongly associated with worse clinical outcomes, while lower SRC transcript levels were independently linked to better survival [31]. Emerging reports also suggest that both the expression and activation of SRC are associated with the emergence of malignant phenotypes and reduced survival in RCC [31, 32]. SRC is considered a promising target for ccRCC therapies. Priyanka et al. reported that miR-155 directly interacts with lncTCL6 in ccRCC, resulting in the activation of the SRC–Akt pathway, which promotes ccRCC metastasis [33]. TRIM7 functions as a tumor suppressor by influencing HIF-1α accumulation through targeting the SRC-triggered PI3K/AKT/mTOR signaling pathway, thereby inhibiting the progression of ccRCC cells [34]. In VHL− or VHL+ 786-O treated cells, simultaneous inhibition of SRC resulted in a significant induction of apoptosis [31]. Furthermore, SRC inhibition not only blocks renal interstitial fibroblast activation but also ameliorates renal fibrosis, indicating that SRC represents a potential therapeutic target for the treatment of chronic renal

fibrosis [35]. Our study observed that elevated levels of SRC in ccRCC were inhibited by *ATP1A1*, suggesting that *ATP1A1* may serve as a target for the SRC signaling pathway in the treatment of ccRCC. Further investigations revealed that *ATP1A1* inhibited the proliferation of ccRCC cells through the inactivation of the SRC signaling pathway, leading to abnormal cellular metabolism.

Moreover, our integrated approach, which combines molecular docking with experimental validation, provides critical evidence for the interaction between *ATP1A1* and SRC. Previous studies have shown that the CD2 domain of the Na^+/K^+-ATPase α1 subunit regulates SRC kinase activity by binding to its SH2 domain [6]. These findings suggest that *ATP1A1* may function as an inhibitor of the SRC pathway in ccRCC, highlighting its potential as a molecular therapeutic target. Elevating *ATP1A1* levels exogenously or administering its analogs could represent a promising therapeutic strategy.

pNaktide, a cell-permeable peptide designed by mapping the site of α1 NKA/SRC binding, has demonstrated broad application potential across various disease models [36]. Research findings indicate that pNaktide has extensive applicability, particularly in mouse models of insulin resistance and glucose intolerance, where it effectively counters metabolic disorders by regulating the SRC pathway [37]. In the LLC-PK1 cell line, pNaktide restored the hydrogen peroxide-activated SRC-ERK1/2 signaling cascade, further validating its significance in cellular signal regulation [38]. Moreover, pNaktide has shown promise in alleviating uremic cardiomyopathy, reducing the risks associated with fatty liver disease and atherosclerosis [39], and slowing cellular senescence [40], thereby expanding its potential clinical applications. In prostate cancer, where *ATP1A1* expression is downregulated, the addition of pNaktide stimulated apoptosis in tumor cells and inhibited tumor angiogenesis, presenting a novel therapeutic approach for this malignancy [41]. In studies focusing on non-alcoholic steatohepatitis (NASH)-related liver cancer, pNaktide effectively normalized α1 NKA signaling, which not only prevented and reversed NASH-related metabolic alterations but also exhibited tumor-suppressive effects [42]. Overall, pNaktide demonstrates significant potential in the treatment of metabolic diseases and cancer through various mechanisms, suggesting that its promise as a therapeutic agent for ccRCC by reversing the signaling pathway dysregulation associated with *ATP1A1* loss, thereby exerting its therapeutic effects. We treated ccRCC cell lines with varying concentrations of pNaktide and observed a significant inhibition of cell proliferation, accompanied by a marked decrease in the activity of the SRC/ERK signaling pathway. This phenomenon was further validated using a nude mouse xenograft model. Additionally, in *ATP1A1*-knockdown 786-O cells, pNaktide was able to restore the inhibition of the SRC signaling pathway, thereby confirming its potential as a therapeutic agent for reversing the dysregulation of the signaling cascade associated with *ATP1A1* downregulation.

pNaKtide is a peptide derivative that mimics the N-terminal domain of the α1 subunit of Na^+/K^+-ATPase, specifically designed to disrupt the formation of the Na^+/K^+-ATPase/SRC complex [43, 44]. While our current findings, along with previous reports, support its role as a pathway-selective modulator of the *ATP1A1*-SRC axis, its molecular specificity and potential off-target effects were not experimentally validated in this study. Future studies will employ CRISPR-Cas9-mediated *ATP1A1* knockout models to directly assess whether the biological effects of pNaKtide are specifically mediated through the *ATP1A1*-SRC axis.

The Warburg effect, characterized by a high rate of glycolysis and lactic acid fermentation even in the presence of sufficient oxygen, is a well-established feature of most cancer cells [45]. Reversing the Warburg effect in tumor cells has been shown to significantly compromise their tumorigenicity, suggesting that targeting these metabolic changes could be an effective strategy for cancer treatment [46]. ccRCC is associated with abnormalities in glucose metabolism and OXPHOS, as well as unique metabolic alterations [47]. Recent evidence indicates that ccRCC may be classified as a metabolic disease. These metabolic alterations provide potential targets for novel therapeutic interventions or biomarkers for monitoring tumor growth and prognosis. By analyzing ccRCC sequencing data from the TCGA database, we identified key genes related to *ATP1A1*. Through PPI analysis, we identified five hub genes: *CLDN7*, *MUC1*, *PPARGC1A*, *OCLN*, and *IRS1*. Among these, *CLDN7* and *MUC1* have been reported to play critical roles in tumor progression, while *PPARGC1A* and *IRS1* are involved in cellular metabolic processes. Further pathway enrichment analysis revealed that the pathways regulated by genes associated with *ATP1A1* are primarily related to cellular metabolism, suggesting that the *ATP1A1* gene may be involved in regulating metabolic processes in ccRCC.

Metabolic studies in mutant cell lines have demonstrated that the SRC-binding regions of α1 NKA are crucial for maintaining metabolic reserves and flexibility [37]. Cell lines with mutations in the α1 NKA/SRC-binding site exhibited reduced mitochondrial metabolism, increased reliance on glycolysis, and diminished metabolic reserves [48]. We hypothesize that ccRCC, *ATP1A1*, regulates tumor growth through its interaction with SRC, targeting cellular metabolic pathways to facilitate this function. To test this hypothesis, we employed mitochondrial stress testing and glycolysis analysis utilizing Seahorse metabolic flux technology. Our study confirmed that in ccRCC cell lines overexpressing *ATP1A1*, glycolysis levels were inhibited while OXPHOS levels were elevated. Furthermore, exogenous pNaktide was able to reverse the metabolic changes induced by *ATP1A1* knockdown. OXPHOS has been identified as a significant source of ROS production. Further studies revealed that ROS levels were significantly upregulated in ccRCC cell lines overexpressing *ATP1A1*. Previous research has shown that ROS sensitizes cells to apoptosis through various mechanisms, with mitochondria serving as the primary source of ROS within cells. The accumulation of ROS resulting from enhanced OXPHOS could activate various cell death pathways. These findings confirm that *ATP1A1* regulates cell metabolism through the SRC signaling pathway, promotes ROS accumulation, and induces apoptotic pathways.

CONCLUSION

In summary, our study suggests that *ATP1A1* holds promise as a prognostic molecular marker for ccRCC and underscores its critical role in the proliferation of ccRCC. Our research elucidates the molecular mechanism by which *ATP1A1* interacts with SRC to influence cellular metabolic pathways, thereby inhibiting the progression of ccRCC. Furthermore, we demonstrate that the *ATP1A1* analog, pNaktide, can reverse SRC pathway activation and metabolic abnormalities induced by *ATP1A1* downregulation, exhibiting significant tumor-suppressive effects. This provides a theoretical basis and potential direction for future molecular drug development targeting *ATP1A1* and the SRC pathway. However, it is important to note that this study was conducted in vitro and in mouse models; clinical trials are necessary to validate the efficacy and safety of pNaktide. Additionally, the specific molecular mechanisms underlying this interaction warrant further investigation.

DATA AVAILABILITY

The datasets generated and analyzed during the current study are available from the corresponding author upon reasonable request.

REFERENCES

1. Ganini C, Montanaro M, Scimeca M, Palmieri G, Anemona L, Concetti L, et al. No time to die: How kidney cancer evades cell death. Int J Mol Sci. 2022;23:6198.
2. Siegel RL, Giaquinto AN, Jemal A. Cancer statistics, 2024. CA Cancer J Clin. 2024;74:12–49.
3. Wettersten HI, Aboud OA, Lara PN Jr, Weiss RH. Metabolic reprogramming in clear cell renal cell carcinoma. Nat Rev Nephrol. 2017;13:410–9.
4. Das P, Booth A, Donaldson R, Berfeld N, Nordstrom B, Carroll R, et al. Patient characteristics, treatment patterns, and outcomes for patients with renal cell carcinoma in england: a retrospective cohort study. Clin Genitourin Cancer. 2024;22:102081.
5. Xie Z, Askari A. Na(+)/K(+)-ATPase as a signal transducer. Eur J Biochem. 2002;269:2434–9.
6. Yu H, Cui X, Zhang J, Xie JX, Banerjee M, Pierre SV, et al. Heterogeneity of signal transduction by Na-K-ATPase α-isoforms: role of Src interaction. Am J Physiol Cell Physiol. 2018;314:C202–10.
7. Mijatovic T, Roland I, Van Quaquebeke E, Nilsson B, Mathieu A, Van Vynckt F, et al. The alpha1 subunit of the sodium pump could represent a novel target to combat non-small cell lung cancers. J Pathol. 2007;212:170–9.
8. Soumoy L, Genbauffe A, Mouchart L, Sperone A, Trelcat A, Mukeba-Harchies L, et al. ATP1A1 is a promising new target for melanoma treatment and can be inhibited by its physiological ligand bufalin to restore targeted therapy efficacy. Cancer Cell Int. 2024;24:8.
9. Feng X, Li J, Li H, Chen X, Liu D, Li R. Bioactive C21 steroidal glycosides from Euphorbia kansui promoted HepG2 cell apoptosis via the degradation of ATP1A1 and inhibited macrophage polarization under co-cultivation. Molecules. 2023;28:2830.
10. Mobasheri A, Fox R, Evans I, Cullingham F, Martín-Vasallo P, Foster CS. Epithelial Na, K-ATPase expression is down-regulated in canine prostate cancer; a possible consequence of metabolic transformation in the process of prostate malignancy. Cancer Cell Int. 2003;3:8.
11. Nakamura K, Shiozaki A, Kosuga T, Shimizu H, Kudou M, Ohashi T, et al. The expression of the alpha1 subunit of Na(+)/K(+)-ATPase is related to tumor development and clinical outcomes in gastric cancer. Gastric Cancer. 2021;24:1278–92.
12. Sumiyoshi S, Shiozaki A, Kosuga T, Simizu H, Kudo M, Kiuchi J, et al. Functional analysis and clinical importance of ATP1A1 in colon cancer. Ann Surg Oncol. 2023;30:6898–910.
13. Kim Y, Ko JY, Kong HK, Lee M, Chung W, Lim S, et al. Hypomethylation of ATP1A1 is associated with poor prognosis and cancer progression in triple-negative breast cancer. Cancers. 2024;16:1666.
14. Zhang D, Zhang P, Yang P, He Y, Wang X, Yang Y, et al. Downregulation of ATP1A1 promotes cancer development in renal cell carcinoma. Clin Proteom. 2017;14:15.
15. Chen B, Jiao Z, Yin X, Qian Z, Gu J, Sun H. Novel insights into biomarkers associated with renal cell carcinoma. Oncol Lett. 2018;16:83–90.
16. Tian J, Cai T, Yuan Z, Wang H, Liu L, Haas M, et al. Binding of Src to Na+/K+-ATPase forms a functional signaling complex. Mol Biol Cell. 2006;17:317–26.
17. Yu Y, Chen C, Huo G, Deng J, Zhao H, Xu R, et al. ATP1A1 integrates AKT and ERK signaling via potential interaction with Src to promote growth and survival in glioma stem cells. Front Oncol. 2019;9:320.
18. Yeatman TJ. A renaissance for SRC. Nat Rev Cancer. 2004;4:470–80.
19. Tang Z, Kang B, Li C, Chen T, Zhang Z. GEPIA2: an enhanced web server for large-scale expression profiling and interactive analysis. Nucleic Acids Res. 2019;47:W556–60.
20. Chandrashekar DS, Bashel B, Balasubramanya SAH, Creighton CJ, Ponce-Rodriguez I, Chakravarthi BVSK, et al. UALCAN: a portal for facilitating tumor subgroup gene expression and survival analyses. Neoplasia. 2017;19:649–58.
21. Kanehisa M, Goto S. KEGG: Kyoto Encyclopedia of Genes and Genomes. Nucleic Acids Res. 2000;28:27–30.
22. Aleksander SA, Balhoff J, Carbon S, Cherry JM, Drabkin HJ, Ebert D, et al. The Gene Ontology knowledgebase in 2023. Genetics. 2023;224:iyad031.
23. Gondran P, Dautry F. Regulation of mRNA splicing and transport by the tyrosine kinase activity of src. Oncogene. 1999;18:2547–55.
24. Zhuang L, Xu L, Wang P, Jiang Y, Yong P, Zhang C, et al. Na+/K+-ATPase α1 subunit, a novel therapeutic target for hepatocellular carcinoma. Oncotarget. 2015;6:28183–93.
25. de Souza WF, Barbosa LA, Liu L, de Araujo WM, de-Freitas-Junior JC, Fortunato-Miranda N, et al. Ouabain-induced alterations of the apical junctional complex involve α1 and β1 Na,K-ATPase downregulation and ERK1/2 activation independent of caveolae in colorectal cancer cells. J Membr Biol. 2014;247:23–33.
26. Feng XY, Zhao W, Yao Z, Wei NY, Shi AH, Chen WH. Downregulation of ATP1A1 expression by Panax notoginseng (Burk.) F.H. Chen Saponins: a potential mechanism of antitumor effects in HepG2 cells and in vivo. Front Pharmacol. 2021;12:720368.
27. Zhang X, Yao Z, Xue Z, Wang S, Liu X, Hu Y, et al. Resibufogenin targets the ATP1A1 signaling cascade to induce G2/M phase arrest and inhibit invasion in glioma. Front Pharmacol. 2022;13:855626.
28. Kester HA, van der Leede BM, van der Saag PT, van der Burg B. Novel progesterone target genes identified by an improved differential display technique suggest that progestin-induced growth inhibition of breast cancer cells coincides with enhancement of differentiation. J Biol Chem. 1997;272:16637–43.
29. He Y, Zhang P, Zhang D, Xia Z, Wang X, Deng S, et al. Combined assessment of low PGRMC1/positive ATP1A1 levels has enhanced prognostic value for renal cell carcinoma. Oncol Rep. 2018;40:1467–76.
30. Kopetz S, Shah AN, Gallick GE. Src continues aging: current and future clinical directions. Clin Cancer Res. 2007;13:7232–6.
31. Roelants C, Giacosa S, Pillet C, Bussat R, Champelovier P, Bastien O, et al. Combined inhibition of PI3K and Src kinases demonstrates synergistic therapeutic efficacy in clear-cell renal carcinoma. Oncotarget. 2018;9:30066–78.
32. Yonezawa Y, Nagashima Y, Sato H, Virgona N, Fukumoto K, Shirai S, et al. Contribution of the Src family of kinases to the appearance of malignant phenotypes in renal cancer cells. Mol Carcinog. 2005;43:188–97.
33. Kulkarni P, Dasgupta P, Hashimoto Y, Shiina M, Shahryari V, Tabatabai ZL, et al. A lncRNA TCL6-miR-155 interaction regulates the Src-Akt-EMT network to mediate kidney cancer progression and metastasis. Cancer Res. 2021;81:1500–12.
34. Yuan C, Liu J, Liu L, Jia H, Gao Q, Wang X, et al. TRIM7 suppresses cell invasion and migration through inhibiting HIF-1α accumulation in clear cell renal cell carcinoma. Cell Biol Int. 2022;46:554–67.
35. Yan Y, Ma L, Zhou X, Ponnusamy M, Tang J, Zhuang MA, et al. Src inhibition blocks renal interstitial fibroblast activation and ameliorates renal fibrosis. Kidney Int. 2016;89:68–81.
36. Wang J, Wang X, Gao Y, Lin Z, Chen J, Gigantelli J, et al. Stress signal regulation by Na/K-ATPase as a new approach to promote physiological revascularization in a mouse model of ischemic retinopathy. Invest Ophthalmol Vis Sci. 2020;61:9.
37. Kutz LC, Cui X, Xie JX, Mukherji ST, Terrell KC, Huang M, et al. The Na/K-ATPase α1/Src interaction regulates metabolic reserve and Western diet intolerance. Acta Physiol. 2021;232:e13652.
38. Wang Y, Ye Q, Liu C, Xie JX, Yan Y, Lai F, et al. Involvement of Na/K-ATPase in hydrogen peroxide-induced activation of the Src/ERK pathway in LLC-PK1 cells. Free Radic Biol Med. 2014;71:415–26.
39. Sodhi K, Srikanthan K, Goguet-Rubio P, Nichols A, Mallick A, Nawab A, et al. pNaKtide attenuates steatohepatitis and atherosclerosis by blocking Na/K-ATPase/ROS amplification in C57Bl6 and ApoE knockout mice fed a Western diet. Sci Rep. 2017;7:193.
40. Sodhi K, Nichols A, Mallick A, Klug RL, Liu J, Wang X, et al. The Na/K-ATPase oxidant amplification loop regulates aging. Sci Rep. 2018;8:9721.
41. Li Z, Zhang Z, Xie JX, Li X, Tian J, Cai T, et al. Na/K-ATPase mimetic pNaKtide peptide inhibits the growth of human cancer cells. J Biol Chem. 2011;286:32394–403.
42. Udoh US, Banerjee M, Rajan PK, Sanabria JD, Smith G, Schade M, et al. Tumor-suppressor role of the α1-Na/K-ATPase signalosome in NASH related hepatocellular carcinoma. Int J Mol Sci. 2022;23:7359.
43. Li Z, Cai T, Tian J, Xie JX, Zhao X, Liu L, et al. NaKtide, a Na/K-ATPase-derived peptide Src inhibitor, antagonizes ouabain-activated signal transduction in cultured cells. J Biol Chem. 2009;284:21066–76.
44. Liu J, Tian J, Chaudhry M, Maxwell K, Yan Y, Wang X, et al. Attenuation of Na/K-ATPase mediated oxidant amplification with pNaKtide ameliorates experimental uremic cardiomyopathy. Sci Rep. 2016;6:34592.
45. Warburg O. On the origin of cancer cells. Science. 1956;123:309–14.
46. Christofk HR, Vander Heiden MG, Harris MH, Ramanathan A, Gerszten RE, Wei R, et al. The M2 splice isoform of pyruvate kinase is important for cancer metabolism and tumour growth. Nature. 2008;452:230–3.
47. Hakimi AA, Reznik E, Lee CH, Creighton CJ, Brannon AR, Luna A, et al. An integrated metabolic atlas of clear cell renal cell carcinoma. Cancer Cell. 2016;29:104–16.
48. Banerjee M, Cui X, Li Z, Yu H, Cai L, Jia X, et al. Na/K-ATPase Y260 phosphorylation-mediated Src regulation in control of aerobic glycolysis and tumor growth. Sci Rep. 2018;8:12322.

ACKNOWLEDGEMENTS

The authors express their gratitude to Professor Xie Zijian from Marshall University for providing the pNaktide. The graphical abstract was created with permission using BioRender (https://biorender.com/).

AUTHOR CONTRIBUTIONS

Yinghong Zhao and Jialing Lv were responsible for data collection, analysis, and the drafting of the manuscript. Wen Zhang, Ruoyu Deng, Chunyan Li, Lin Wang, and Tengfei Zhang contributed to the experiments and the interpretation of the data. Feineng Liu assisted with statistical analysis and visualization. Kaili Ma and Zhengcun Wu provided supervision, project management, and revisions of the manuscript. Chao Zhang designed the study, coordinated the research efforts, and finalized the manuscript.

FUNDING

This work was supported by the Natural Science Foundation of Yunnan Province (Grant number: 202301AT070361); High level Science and Technology Talents Foundation of Yunnan province (Grant number:202305AD350030); Yunnan Science and Technology Department and Kunming Medical University (Grant number: 202301AY070001-057); National Clinical Key Specialty Construction Project (Grant number: Z155080000004) and Yunnan Provincial Department of Education Science Research Fund Project (Grant number:2024Y917).

COMPETING INTERESTS

The authors declare no competing interests.

ETHICS APPROVAL AND CONSENT TO PARTICIPATE

All animal experimental procedures were approved by the Ethics Committee of Kunming Medical University (Approval No: KMMU20221136) and were conducted in accordance with institutional guidelines and relevant regulations. No human participants or clinical samples were involved in this study; therefore, informed consent and trial registration were not applicable.

ADDITIONAL INFORMATION

Supplementary information The online version contains supplementary material available at https://doi.org/10.1038/s41417-025-00971-z.

Correspondence and requests for materials should be addressed to Kaili Ma, Zhengcun Wu or Chao Zhang.